PROCEEDINGS OF SCIENCE

Measurement of the Proton Spectrum with CALET on the ISS

Pier Simone Marrocchesi *
Dept.of Physical Sciences, Earth and Environment, Univ. of Siena, 53100 Siena, Italy
E-mail: marrocchesi@pi.infn.it, *for the CALET Collaboration*†

The CALorimetric Electron Telescope CALET on the International Space Station has been collecting science data since mid October 2015 with excellent performance and no significant interruptions. In addition to its primary goal of exploring the electron spectrum in the poorly known energy region above 1 TeV, CALET is investigating the hadronic component of cosmic rays with direct measurements of the energy spectra, relative abundances and secondary-to-primary ratios of elements from proton to iron and above (up to atomic number Z=40). Equipped with a thick (30 X_0 and $\sim$1.3 λ_I) calorimeter, comprised of a finely segmented 3 X_0 pre-shower section with imaging capabilities followed by a 27 X_0 homogeneous calorimeter, and with two independent sub-systems to identify the charge of the incident particle, CALET has an excellent energy and angular resolution and electron/proton discrimination of order 10^{-5}. For the first time CALET covered, with a single instrument, the whole energy interval (from a few tens GeV to the multi-TeV region) previously investigated in separate sub-ranges by magnetic spectrometers and calorimetric instruments. The observation of the proton differential spectrum confirms a deviation from a simple power-law, as previously reported by other experiments. In this paper, the proton spectrum measured by CALET is presented and details of the analysis are given.

36th International Cosmic Ray Conference -ICRC2019-
July 24th - August 1st, 2019
Madison, WI, U.S.A.

*Speaker.
†for collaboration list see PoS(ICRC2019)1177

PoS(ICRC2019)103

1. Introduction

CALET is a space mission led by the Japanese Space Agency (JAXA) with the participation of the Italian Space Agency (ASI) and NASA. It was launched on August 19, 2015 with the Japanese carrier H-II, delivered to the ISS by the HTV-5 Transfer Vehicle, and installed (Fig.1(a)) on the Japanese Experiment Module Exposure Facility (JEM-EF). The CALET science program addresses several outstanding questions of high-energy astroparticle physics including the origin of cosmic rays (CR); the possible presence of nearby astrophysical CR sources; the study of their acceleration mechanism(s); the propagation of primary and secondary elements in the galaxy; the nature of dark matter and its localization. The design of the CALET instrument [1, 2] has been optimized for high precision measurements of the electron spectrum allowing an accurate scan of the energy interval already covered by previous experiments [3] and its extension to the unexplored region above 1 TeV. Given the high energy resolution of CALET, a detailed study of the spectral shape might reveal the presence of nearby sources of acceleration as well as possible indirect signatures of dark matter. The CALET collaboration reported their first measurement of the inclusive electron+positron spectrum in the energy range from 10 GeV to 3 TeV [4] with a selection of events falling into a subset of the total acceptance. It was followed by a second paper [5] reporting an electron analysis with higher statistics (780 days of flight data) within the full geometrical acceptance and with an extended energy range to 4.8 TeV.

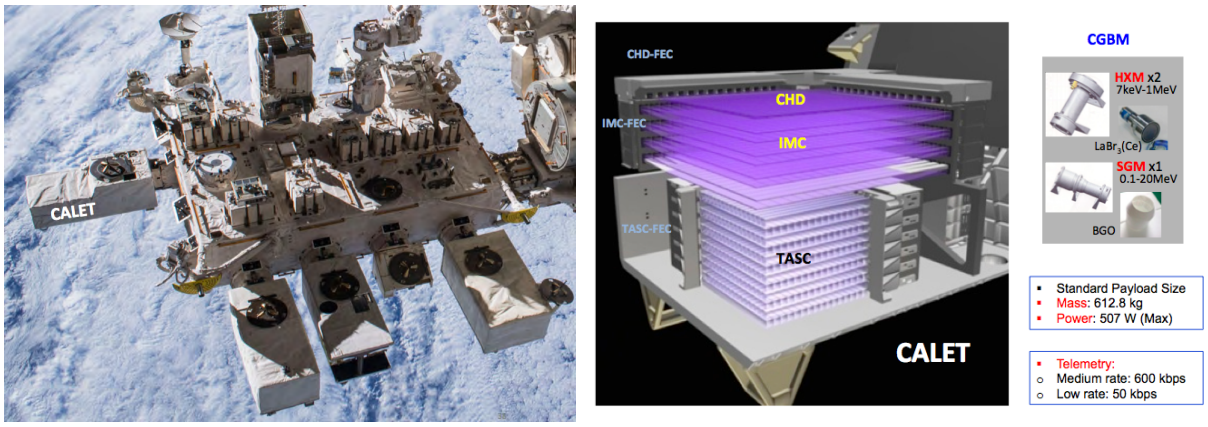

(a) (b)

Figure 1: (a) CALET on the JEM-EF; (b) Layout of the CALET instrument and of the Gamma-Ray Burst Monitor (CGBM)

Taking advantage of its capability of identifying cosmic rays with individual element resolution, CALET is also carrying out direct measurements of the spectra and relative abundances of light and heavy cosmic nuclei [6, 7] from proton to iron in the energy range from a few tens of GeV to several hundred TeV. The abundances (normalized to Iron) of trans-iron elements up to $Z\sim40$ are studied with a dedicated program of long term observations [8].

CALET can identify gamma-rays and measure their energies from $\sim$1 GeV to the TeV region with an angular resolution $< 2^\circ$ above 1 GeV ($< 0.2^\circ$ above 10 GeV). Measured signals from gamma-ray bright point sources and diffuse galactic emission were found to be in agreement with simulated results and expectations based on Fermi-LAT data [9]. Gamma-ray transients are detected by a dedicated instrument (CGBM) covering the energy range 7 keV–20 MeV. Combined analyses of CGBM and calorimeter were performed for the search of counterpart emission related to gravitational wave events. More detailed information on these studies can be found in [10, 11].

In this paper, we report the recent direct measurement of the proton spectrum by CALET in the energy range from 50 GeV to 10 TeV after 3 years of operations on the ISS and discuss some aspects of the analysis of the data. We also summarize the present status of available direct spectral measurements of high energy protons performed by instruments on balloons and in space.

2. CALET (CALorimetric Electron Telescope)

The CALET instrument (Fig 1(b)) includes a thick calorimeter, designed to achieve shower containment and a large proton rejection capability ($>10^5$), which is longitudinally segmented into a fine grained imaging calorimeter (IMC) followed by a total absorption calorimeter (TASC). The overall thickness of CALET at normal incidence is 30 X_0 and $\sim$1.3 proton interaction length (λ_I). The charge identification of individual nuclear species is performed by a two-layered hodoscope of plastic scintillators (CHD), positioned at the top of the apparatus, providing a measurement of the charge Z of the incident particle over a wide dynamic range ($Z = 1$ to ~ 40) with sufficient charge resolution to resolve individual elements [12] and complemented by a redundant charge determination via multiple dE/dx measurements in the IMC. The latter is a sampling calorimeter segmented longitudinally into 16 layers of scintillating fibers (with 1 mm^2 square cross-section) readout individually and interspaced with thin tungsten absorbers. Alternate planes of fibers are arranged along orthogonal directions. It can image the early shower profile in the first 3 X_0 and reconstruct the incident direction of cosmic rays with good angular resolution (0.1° for electrons and better than 0.5° for hadrons) [1, 3]. The TASC is a 27 X_0 thick homogeneous calorimeter with 12 alternate X-Y layers of lead-tungstate (PWO) logs. It measures the total energy of the incident particle and discriminates electrons from hadrons with the help of the information from the CHD and IMC. The geometrical factor of CALET is $\sim$ 0.1 m^2sr and the total weight is 613 kg. The instrument is described in more detail elsewhere [1, 13].

3. CALET Proton Analysis

In the analysis reported here, the reconstructed events are accepted only within a fiducial region, known as Acceptance-A, limited to a geometric factor of $\sim$ 0.042 m^2 sr (about 40% of the total GF) where instrument edge effects do not affect significantly the result. Selection criteria are optimized using MC simulations with protons, helium and electrons samples and applied in an identical way to both Flight (FD) and MC data (MC). A preselection of well reconstructed and well contained events is first performed on the basis of the following criteria.

(1) Offline trigger confirmation – Since the onboard High Energy (HE) trigger can be affected by position and temperature dependence as well as temporal gain variations, an offline trigger is applied requiring sufficiently severer conditions than the onboard HE trigger. When analyzing events triggered by low-energy (LE) trigger [1] the offline trigger confirmation uses lower thresholds. More details can be found in [14]. **(2) Geometrical condition** – A reconstructed track contained in Acceptance A is required to pass through the whole detector, i.e., from CHD top to TASC bottom, with 2 cm clearance from the sides of the TASC. **(3) Track quality cut** – Tracks are reconstructed using a Combinatorial Kalman Filter (KF) tracking algorithm [15] using IMC position information. A fit of the shower axis is performed independently in the TASC and it is used to define a ROI (Road Of Interest) around its direction to reduce the combinatorial in IMC. Track quality criteria and a χ^2 cut are applied in both projections. **(4) Electron background rejection** – A fractional quantity, known as Moliere concentration, is calculated summing all energy deposits found inside one Moliere radius ($\pm$9 fibers) around each fiber matched to the track and then dividing by the total energy deposit sum in IMC. By requiring this quantity to be less than 0.7, most of electrons are rejected while retaining a very high efficiency for protons. **(5) Off-acceptance events rejection** – Off-acceptance events are defined as those erroneously reconstructed as Acceptance A while the true acceptance is different. The maximum fractional energy deposit in a single TASC layer is required to be less than 0.4 to reject laterally incident tracks. The maximum energy deposit ratio of the edge logs in the TASC to the maximum log in each layer is also required to be less than 0.4. The latter cut is effective in removing events exiting from the sides of TASC.

[1] a dedicated Low Energy trigger (LE) is in place to study electron energies down to about 1 GeV.

(6) Track consistency with TASC energy deposit – In order to further reject mis-reconstructed events, a consistency cut is defined between the impact points of a track onto the first two layers of the TASC and the centers of gravity of the corresponding energy deposits. Energy dependent thresholds are defined using MC simulation to achieve a constant efficiency of 95% for events (hereafter denoted as "target" events) that interacted in IMC below the 4th layer and are suitable for determining charge, energy, and trigger efficiency. **(7) Shower development requirement in IMC** – The energy deposit sum of ± 9 fibers along the shower (in total 19 fibers) axis is used to ensure the existence of a shower core in IMC. Energy dependent thresholds are defined to get 99% efficiency for "target" events.

3.1 Combined charge identification with CHD and IMC

The identification of protons and cosmic nuclei via a measurement of their charge is carried out in CALET with two independent subsystems that are routinely used to cross-calibrate each other: the CHD and the IMC. The latter, being equipped with individually readout scintillating fibers, has a suitable granularity to provide excellent tracking capabilities [15] and to sample the ionization deposits in each layer thereby providing a multiple dE/dx measurement with a maximum of 16 samples along the track. The interaction point (IP) is first reconstructed [16] and only the dE/dx ionization clusters from the layers upstream the IP are used. The charge value is evaluated as the truncated-mean of the valid samples with a truncation level set at 70%. The non-linear response due to the saturation of the scintillation light in the fibers is corrected for by fitting the light yield according to the *halo* model of [17, 18]. After application of position and time-dependent

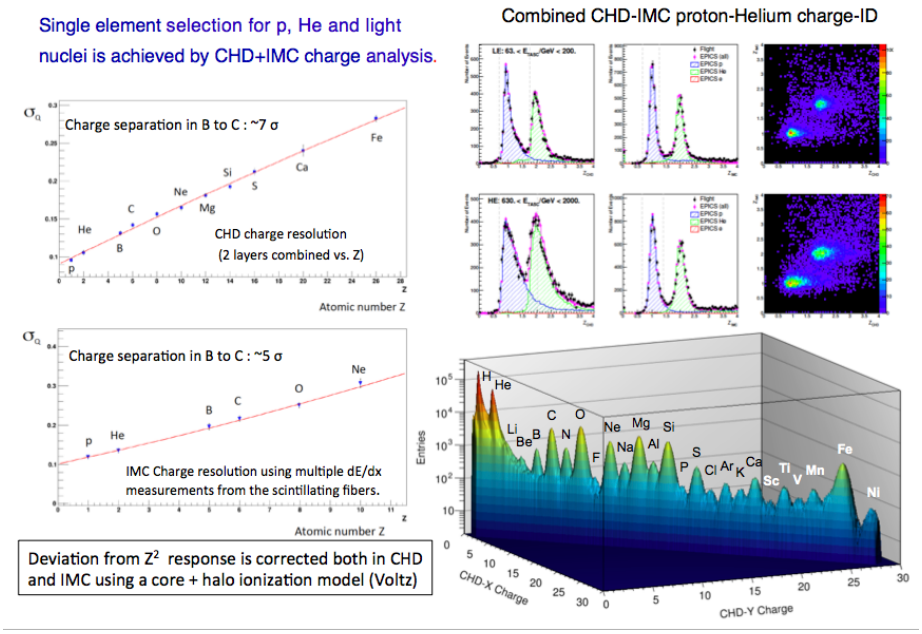

Figure 2: Top left panel: CHD charge resolution for elements from proton to iron; Bottom left panel: IMC charge resolution (proton to neon); Correlation plots of CHD vs IMC charge are shown: (i) for proton and helium candidates (top right panels) (ii) for elements from proton to nichel (bottom right panel)

calibrations and corrections for each CHD paddle [13] the information from the two CHD layers is combined into a single charge estimator. The overall CHD charge resolution (in Z units) is then plotted in Fig.2(a) showing a linear increase as a function of the atomic number from <0.1 for protons to ~ 0.3 for iron. For the IMC, although the photostatistics available at single fiber level is about one order of magnitude lower than a single CHD layer, the charge measurement – thanks to the multiple sampling – achieves an adequate performance as shown in Fig.2(b) where

the IMC charge resolution is plotted as a function of atomic number Z. Charge selection of proton and helium candidates is performed by applying simultaneous window cuts on CHD and IMC reconstructed charges.

3.2 Background Contamination

Background contamination is estimated from the MC simulation of protons, helium and electrons as a function of the observed energy. Available spectral data, e.g. from AMS-02 [19, 20] and CREAM-III [21], are used to simulate their spectral shape. The dominant component is off-acceptance protons except for the highest energy region $E_{\mathrm{TASC}} \sim 10$ TeV where helium contamination becomes dominant. The overall contamination is estimated below a few percent with maximua $\sim$5% in the lowest and highest energy regions. Background subtraction is applied before performing the energy unfolding procedure. In the lower energy region, the mis-reconstruction probability for protons is higher, due to the poorer reconstruction of the TASC shower axis caused by the less prolate shower shape at these energies. For helium, this probability is much lower due to the larger energy deposits in each hit produced by a primary track in IMC. This is the main reason behind the higher contamination ratio due to off-acceptance protons in the low energy region (LE). In the higher energy region (HE) above 1 TeV, the effect of backscattering gets increasingly significant, therefore the helium dominates the total contamination at the highest energies although sufficiently small not to significantly affect the proton spectrum.

4. Energy Calibration and absolute energy scale

For an all-calorimetric instrument like CALET, energy calibrations are essential to achieve accurate flux measurements. The calibration procedures described in [13] establish the values of the ADC-to-deposited-energy conversion factors, enforce a linear energy response over each gain range (TASC has four gain ranges for each channel), and provide a seamless transition among neighboring ranges. The calibration of the lower gain interval is particularly important for spectral measurements in the TeV range. Position and temperature dependence as well as temporal gain variations are corrected for [13]. Linearity of the response was first established during pre-flight tests on ground with laser beam illumination of individual TASC logs. In flight runs with not interacting helium tracks for calibration are routinely performed with a dedicated onboard trigger. An assessement of the absolute energy scale for protons using the geomagnetic rigidity cutoff could not be performed as in the case of electrons (as described in [4]) because of the limited energy resolution for protons. The absolute energy-scale had to be inferred from pre-flight beam test measurements that were performed at CERN-SPS. The maximum energy available for protons does not exceed 400 GeV, therefore dedicated beam tests were performed during several campaigns using beam fragments produced by the collision of a primary SPS ion beam (Ar) with an internal target. Nuclear fragments with energies up to 150 GeV/A (mostly selected with the ratio A/Z =2) were used to assess the linear response of the calorimeter up to $\sim$ 5 TeV.

Energy Unfolding – As the observed energy fraction for proton is around 35% and in order to take into account the relatively limited energy resolution for protons (30–40% in the energy interval covered by the above measurements) energy unfolding is applied to correct for bin-to-bin migration effects. An energy unfolding method based on the Bayesian approach and implemented in the RooUnfold package in ROOT was adopted. The response matrix is derived from MC simulations.

5. Systematic Uncertainties

Dominant sources of systematics uncertainties in proton analysis can be grouped into energy independent and energy dependent contributions. The former include systematic effects in normalization and were studied for the electron analysis [4]. This uncertainty is estimated as 4.1% via the sum in quadrature of the uncertainties on live time (3.4%), radiation environment (1.8%),

and long-term stability (1.4%). **(i) Hadronic interaction** – The uncertainty in the hadronic interaction affects directly the trigger efficiency and it is also closely connected to the uncertainty in the energy response. In the low-energy region, the absolute calibration of the trigger efficiency was performed at the beam test. The main source of uncertainty comes from the accuracy of the calibration. Possible systematic bias due to normalization in the measurements of trigger efficiency was considered as a systematic uncertainty and estimated as 2.2% and 3.3% for HE and LE analyses, respectively. In the high-energy region, a non-trivial extrapolation from the maximum available beam energy (400 GeV) is necessary. To address this uncertainty, as well as backscattering modelling and energy response, the relative differences [2] between different MC simulations e.g.: FLUKA and Geant4 versus EPICS. **(ii) Energy response** – As in the case of the uncertainty on the trigger efficiency, the absolute calibration of the energy response was performed using the beam test data in the low-energy region. The main source of uncertainty in the energy response comes from the accuracy of the calibration, with dominant contributions from the uncertainty on temperature measurements during the beam test of $\pm 0.5^o$, which translates into 2.8% energy scale uncertainty. **(iii) Track reconstruction and acceptance** – Tracking can affect many aspects of the analysis including acceptance and charge selection. The effects on the flux are evaluated by studying its dependence on pre-selection cuts relative to goodness-of-tracking. To investigate the uncertainty on the acceptance, restricted acceptance regions have been studied and the resultant fluxes compared. Negligible differences were found. Efficiencies for cut (6) and cut (7) were varied and the relative differences with respect to the reference cases were considered as systematic uncertainty for each energy bin. **(iv) Charge identification** – It is very important to study the flux stability against charge cut efficiencies (Fig. 3), considering that helium contamination may depend on the same cuts and it is one of the main uncertainties in the high energy region. The variations against the charge cut efficiency are included in the systematic uncertainty. **(v) Total systematic uncertainty** – The blue long-dashed and red solid lines of Fig.3 show the total systematic uncertainty for LE and HE analyses, respectively, as a function of primary energy. A breakdown of the individual energy dependent systematic uncertainties in LE and HE analyses can be found in [22].

6. Direct measurements of the proton spectrum

Proton energies from GeV to the multi-TeV region (Fig.4) have been explored – in most cases in separate subranges – by both magnetic spectrometers (BESS-TeV, PAMELA, and AMS-02) and calorimetric instruments (ATIC, CREAM, and NUCLEON). In the intermediate energy region from 200 GeV to 800 GeV a deviation from a single power-law has been observed for both proton and helium spectra by CREAM [21, 23, 24], PAMELA [25, 26] and confirmed with high statistics measurements by AMS-02 [19]. The recent observations by AMS-02, in the region below maximum detectable rigidity (MDR) of a few TV, clearly show that primary elements (like helium, carbon and oxygen) have a very similar rigidity dependence above $\sim$60 GV and that secondary elements (like Li, Be and B) also share an almost identical dependence, albeit different from the primaries. While the latter behavior could probably be attributed to propagation effects (secondaries propagate first as primaries and then as secondaries) it is very important to investigate with high accuracy the energy dependence of the spectral index by extending the presently available measurements to the multi-TeV region. Taking advantage of its large dynamic range, CALET has been able to cover the whole interval of proton energies from 50 GeV to 10 TeV with a single space-borne instrument. This is of particular relevance because CR flux measurements are well known to be affected by relatively large systematic errors often specific of each instrument. The proton flux was extracted from the data collected from October 13, 2015 to August 31, 2018 (1054 days) on the ISS using only 40% of the total acceptance. CALET observations (Fig.4)(a) are consistent with AMS-02

[2]The difference between DPMJET-III (reference) and EPOS was also studied, but it was found to be completely negligible in the energy range considered here, mainly because the use of EPOS is allowed only above 20 TeV.

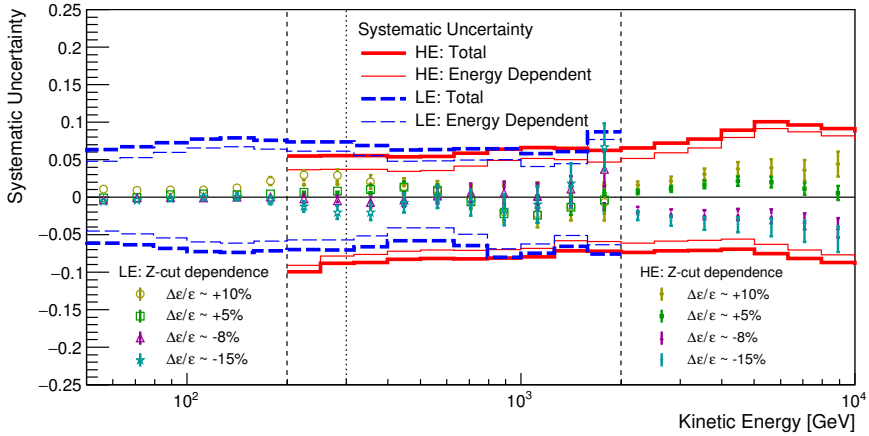

Figure 3: Energy dependence of the total systematic uncertainty band (thick lines). Contributions from energy dependent systematic uncertainty are shown as thinner lines of the same color. Blue long-dashed lines and red solid lines correspond to LE- and HE-trigger analyses, respectively. The total uncertainty is the quadratic sum of energy dependent and normalization uncertainties. The upper (lower) bound of the energy region used in LE (HE) analysis is the dashed line on the left (right) side of the picture. The two analyses are combined at 300 GeV as indicated by the dotted line.

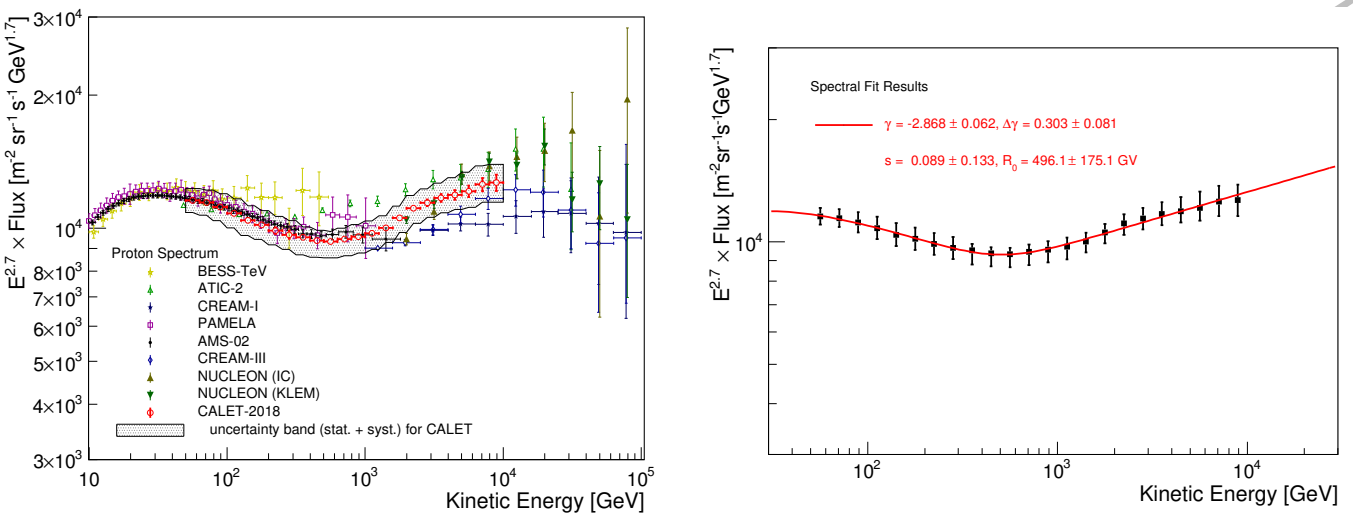

(a) (b)

Figure 4: (a) Cosmic-ray proton spectrum measured by CALET from 50 GeV to 10 TeV using an energy binning of 10 bins per decade. The gray band indicates the quadratic sum of statistical and systematic errors. Also plotted are recent direct measurements in space and from high altitude balloons [19, 27, 24, 21, 28, 29, 30, 31] (b) Fit of the CALET proton spectrum with a smoothly broken power-law function as defined in Eq. (3) of Ref. [19]. Statistical errors are shown in quadrature with systematic errors including only energy dependent ones, neglecting to first order possible correlations among different sources of systematic errors and assuming that they are normally distributed. The fit parameters are given in the plot.

but extend to nearly one order of magnitude higher in energy, showing a very smooth transition of the power-law spectral index from -2.81 ± 0.03 (50–500 GeV) neglecting solar modulation effects (or -2.87 ± 0.06 when including solar modulation effects in the lower energy region) to -2.56 ± 0.04(1–10 TeV), thereby confirming the existence of a spectral hardening and providing evidence of a deviation from a single power law by more than 3σ. The softer value of the spectral index obtained in the smooth fit of (Fig.4)(b) with respect to the single power-law fit in the 50-500 GeV energy interval (details in [22]) is mainly due to the inclusion of a solar modulation potential of 550 MV (fixed) using the force field approximation. The stability of the result versus the choice

of the potential has been studied by varying its value from 450 MV to 650 MV. It has been found to be insensitive within errors, differing at most by 0.01 for γ and $\Delta\gamma$. The available experimental data on proton spectrum above 10 TeV (Fig.4) are at present affected by large statistical and systematic errors. The acceleration limit of supernova remnants calculated with nominal parameters is typically found to be far smaller than the energy of the "knee" and possible Z-dependent (or A-dependent) cutoffs in the spectra of nuclei are hypothesized. According to some models (e.g. [32, 33]) a flux reduction for protons and helium might be expected at rigidities as low as tens of TV. Therefore, precise direct observation of proton and helium spectra in the multi-TeV energy region are of extreme interest. However, exploring this uncharted territory requires a good control of the systematc errors, a requirement that challenges our present knowledge of hadronic interactions, backscattering and energy scale assessment at these very high energies.

7. Summary

An analysis based on a sub-sample of the data collected during the first 3 years aboard the ISS has shown the capability of CALET to extend by about one order of magnitude the energy reach of direct measurements of the proton spectrum provided by magnetic spectrometers. Given the so far excellent performance and the outstanding quality of the data, a steady increase of the available statistics and a more refined understanding of the instrument and of the systematic uncertanties are expected. The CALET mission has been extended to five (or more) years.

References

[1] S. Torii et al., *Proceedings of Science* (ICRC2015) **1092**, 2017
[2] Y. Asaoka for the CALET collaboration, *Proc. of the 36th ICRC (Madison), 2019*
[3] S. Torii for the CALET collaboration, *Proc. of the 36th ICRC (Madison), 2019*
[4] O. Adriani et al. (CALET Collaboration), Phys. Rev. Lett. 119, **181101**, 2017
[5] O. Adriani et al. (CALET Collaboration), Phys. Rev. Lett. 120, **261102**, 2018
[6] P. S. Marrocchesi, *arXiv:1704.00304 [astro-ph.HE]*, 2017
[7] Y. Akaike for the CALET collaboration, *Proc. of the 36th ICRC (Madison), 2019*
[8] B. F. Rauch for the CALET collaboration, *Proc. of the 36th ICRC (Madison), 2019*
[9] N. Cannady et al., *Astrophys. J. Suppl.*, **238**, 2018
[10] O. Adriani et al., ApJ 863, **160**, 2018
[11] M. Mori, Y. Asaoka et al. (CALET Collaboration), *Proc. of the 36th ICRC (Madison), 2019*
[12] P. S. Marrocchesi et al., Nucl. Instr. Meth. A **659**, **477-483**, 2011
[13] Y. Asaoka et al., *Astropart. Phys.* **91**, 1, 2017
[14] Y.Asaoka, S.Ozawa, S.Torii et al., Astropart. Phys. 100 **29-37**, 2018
[15] P. Maestro and N. Mori, *Proc. of the 35th ICRC (Busan, Korea), 2017*
[16] P. Brogi et al., *Proc. of the 34th ICRC (The Hague, Netherlands), 595, 2015*
[17] R. Dwyer et al., Nuclear Instruments and Methods in Physics Research A242 **171-176**, 1985
[18] G. Tarle et al., Nuclear Instruments and Methods in Physics Research B6 **504-512**, 1985
[19] M. Aguilar et al., *Phys. Rev. Lett.* **114**, 171103, 2015
[20] M. Aguilar et al., *Phys. Rev. Lett.* **115**, 211101, 2015
[21] Y. S. Yoon et al., *Astrophys. J.* **839**, 5, 2017
[22] O. Adriani et al. (CALET Collaboration), Phys. Rev. Lett. 122, **181102**, 2019
[23] H. S. Ahn et al., *Astrophys. J.* **714**, 89-93, 2010
[24] Y. S. Yoon et al., *Astrophys. J.* **728**, 122, 2011
[25] O. Adriani, et al., *Science* **332**, 69, 2011
[26] O. Adriani, et al., *Astrophys. J.* **765**, 91-98, 2013
[27] A. Panov et al., Bull. Russ. Acad. Sci. Phys. 71, **494**, 2007
[28] E. Atkin et al., JETP Letters 108, **5**, 2018
[29] S. Haino et al., Phys. Lett. B 594, **35**, 2004
[30] O. Adriani et al., Phys. Rept. 544, **323**, 2014
[31] O. Adriani et al., Riv. Nuovo Cim. 40, **1**, 2017
[32] V. I. Zatsepin and N. V. Sokolskaya, Astronomy Astrophysics 458, **1-5**, 2006
[33] A. A. Lagutin et al, J.Phys. Conf. Ser. 1181, **012023**, 2019